

Electronic Supporting Information

**Stable Supramolecular Porphyrin@Albumin Nanoparticles for
Optimal Photothermal Activity**

Xiaohua Zheng,^{a,b} Lei Wang,^a Zhitao Lei,^c Qing Pei,^{a,b} Shi Liu,^a and Zhigang Xie^{*,a,b}

^aState Key Laboratory of Polymer Physics and Chemistry, Changchun Institute of Applied Chemistry, Chinese Academy of Sciences, Changchun 130022, P. R. China

E-mail: xiez@ciac.ac.cn

^bUniversity of Science and Technology of China, Hefei 230026, PR China

^cCollege of Environmental and Chemical Engineering, Yanshan University, 438 Heibei Avenue, Qinhuangdao, Hebei 066004, P. R. China

Table of contents

Measurements

Fig. S1 Synthesis of alkane chain with different lengths bonded porphyrins.

Fig. S2 (A) ^1H NMR spectrum of TPP-C₂ in CDCl₃. (B) MALDI-TOF mass spectrum of TPP-C₂.

Fig. S3 (A) ^1H NMR spectrum of TPP-C₄ in CDCl₃. (B) MALDI-TOF mass spectrum of TPP-C₄.

Fig. S4 (A) ^1H NMR spectrum of TPP-C₆ in CDCl₃. (B) MALDI-TOF mass spectrum of TPP-C₆.

Fig. S5 (A) ^1H NMR spectrum of TPP-C₈ in CDCl₃. (B) MALDI-TOF mass spectrum of TPP-C₈.

Fig. S6 (A) ^1H NMR spectrum of TPP-C₁₂ in CDCl₃. (B) MALDI-TOF mass spectrum of TPP-C₁₂.

Fig. S7 (A) ^1H NMR spectrum of TPP-C₁₆ in CDCl₃. (B) MALDI-TOF mass spectrum of TPP-C₁₆.

Fig. S8 (A) TEM image and (B) Size distribution of TPP-C₁₆ NPs. (C) The stability and PDI of TPP-C₁₆@HSA SNPs with different ratios of TPP-C₁₆/HSA.

Table S1 The particle size, PDI, and Zeta potential of different TPP-C_n@HSA SNPs.

Fig. S9 DLS change profiles of TPP-C₁₆@HSA SNPs in (A) water (B) FBS (C) water containing 10% FBS for 14 days.

Fig. S10 2D NOESY spectra of TPP-C₁₆@HSA (A) and HSA (B) in D₂O at 298K with a mixing time of 400 ms.

Fig. S11 The calculated photothermal conversion efficiency (PCE) results of TPP-C_n@HSA under the same conditions.

Fig. S12 *In vitro* cytotoxicity of TPP-C₁₆ NPs against (A) L929 cells without irradiation, (B) HeLa, (C) HepG2 and (D) U14 cells with or without laser irradiation (638 nm, 0.9 W cm⁻², 5 min).

Table S2 IC₅₀ Values of TPP-C₁₆ NPs and TPP-C₁₆@HSA SNPs against HeLa, HepG2 and U14 Cells.

Fig. S13 The cell viability after incubated with TPP-C_n@HSA SNPs and treated (A) without irradiation or (B) with laser irradiation.

Fig. S14 (A) Hemolytic activity of different concentration of TPP-C₁₆@HSA SNPs. (B) The blood circulation of TPP-C₁₆@HSA SNPs and TPP-C₁₆ NPs at different time points after intravenous injection (n = 5). The area under curve (AUC) of TPP-C₁₆ NPs and TPP-C₁₆@HSA SNPs are 93.42 and 164.3, respectively. (C) The concentration of TPP-C₁₆ in the main organs and tumors at different time points after intravenous injection of TPP-C₁₆@HSA SNPs. Error bars represent standard deviation (n = 3). (D) The tumor inhibition rates (TIR) and (E) body weight changes of mice from different groups.

Fig. S15 (A) H&E staining photos of tumor slices in different groups made by a microscope. (B) H&E staining pictures of the main organ slices obtained from the seven groups. Scale bars: 100 μ m.

Measurements

Nuclear magnetic resonance hydrogen spectrum (^1H) were recorded at room temperature on a Bruker NMR -400 DRX spectrometer. The sample mass spectrometry (MS) is obtained by the German company Bruker autoflex III intelligent beam mass spectrometer (MALDI-TOF/TOF). The size and size distribution of nanoparticles is determined by the Malvern Zeta-sizer Nano for dynamic light scattering (DLS). The fluorescence spectra were obtained by using PerkinElmer LS-55 Spectrofluorophotometer. UV-Vis absorption spectra were monitored by a Shimadzu UV-2450 PC UV-Vis spectrophotometer. The IR thermal imaging camera is purchased from the FLIR Systems, Inc. with an IR lens of 6.8 mm.

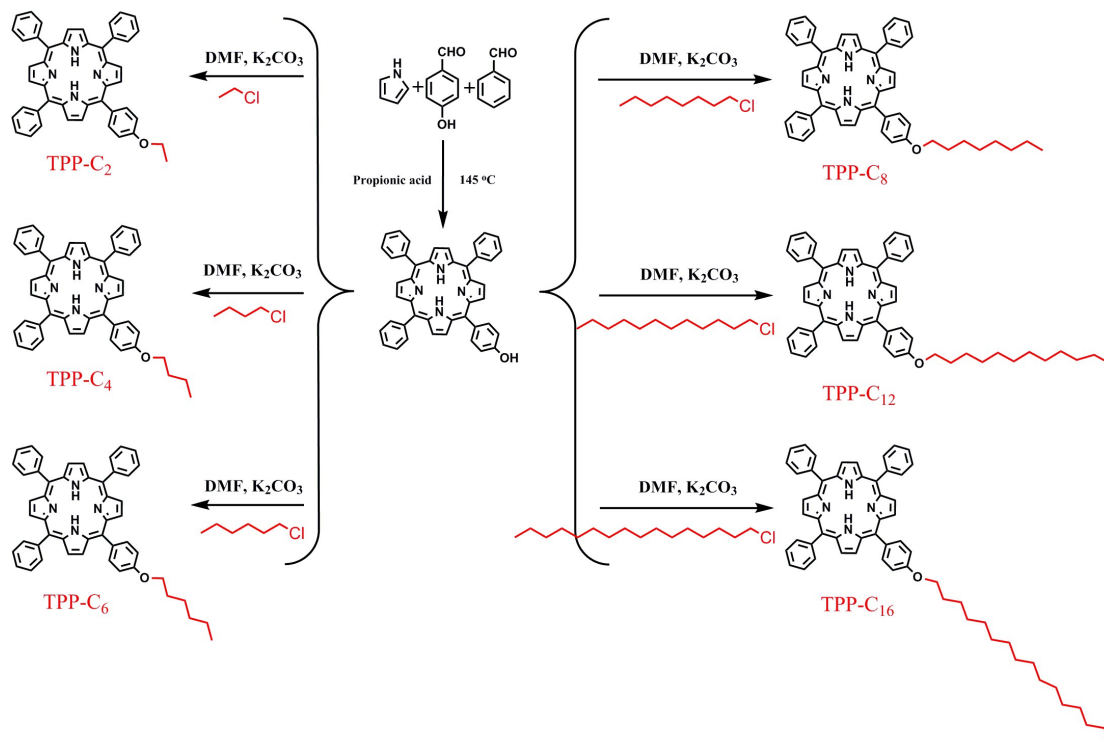


Fig. S1 Synthesis of alkane chain with different lengths bonded porphyrins.

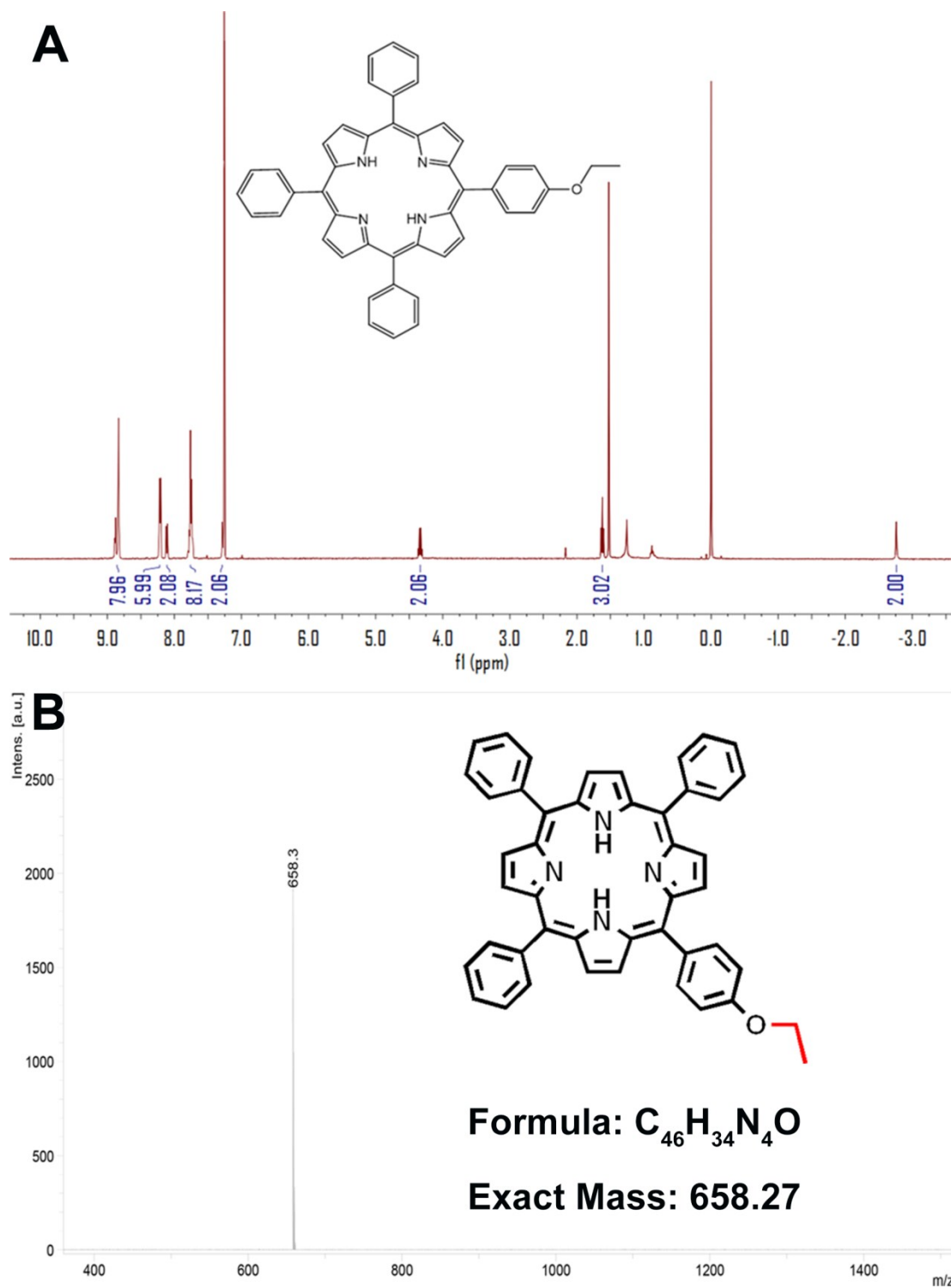


Fig. S2 (A) 1H NMR spectrum of TPP- C_2 in $CDCl_3$. (B) MALDI-TOF mass spectrum of TPP- C_2 .

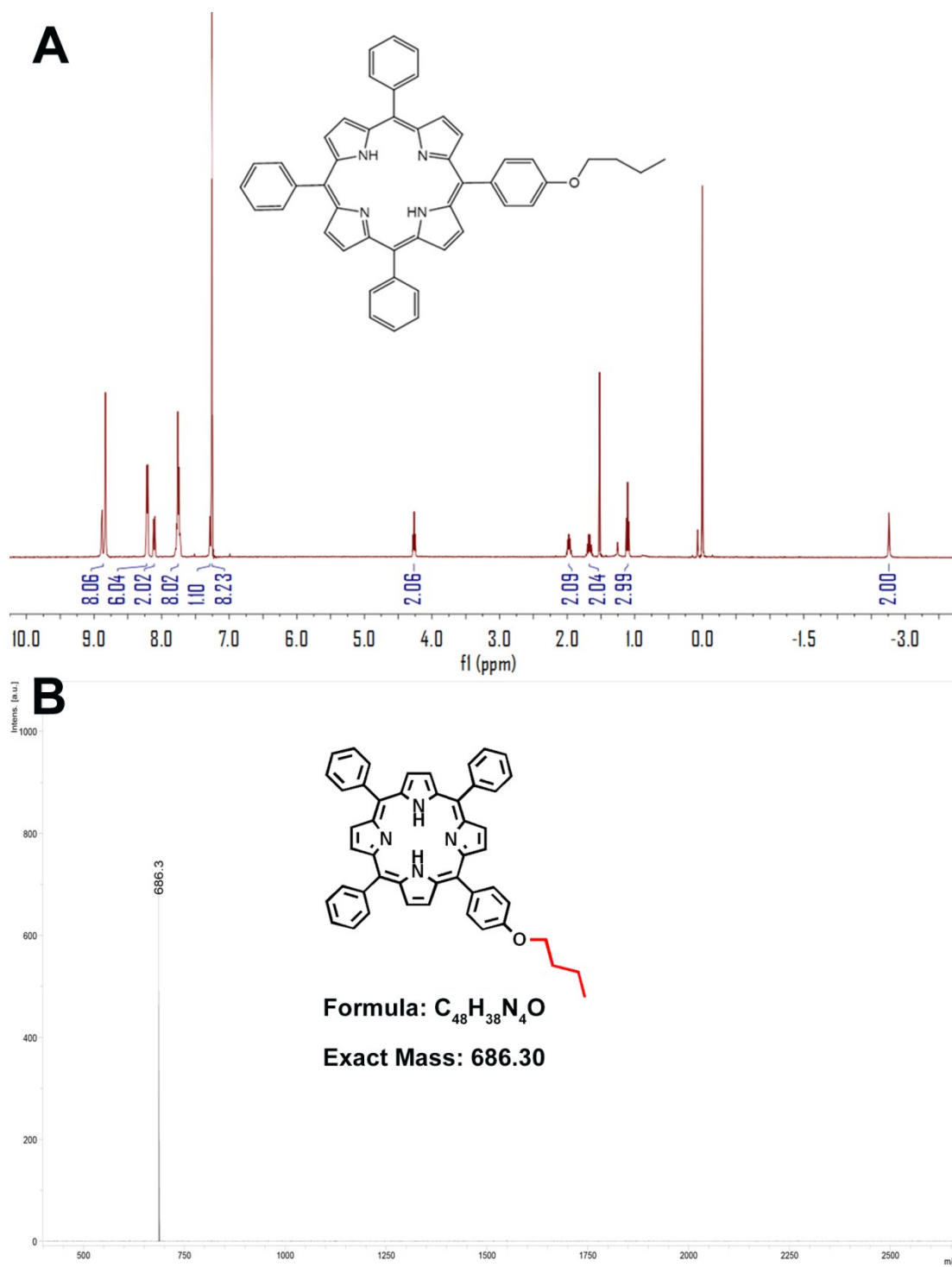


Fig. S3 (A) ¹H NMR spectrum of TPP-C₄ in CDCl₃. (B) MALDI-TOF mass spectrum of TPP-C₄.

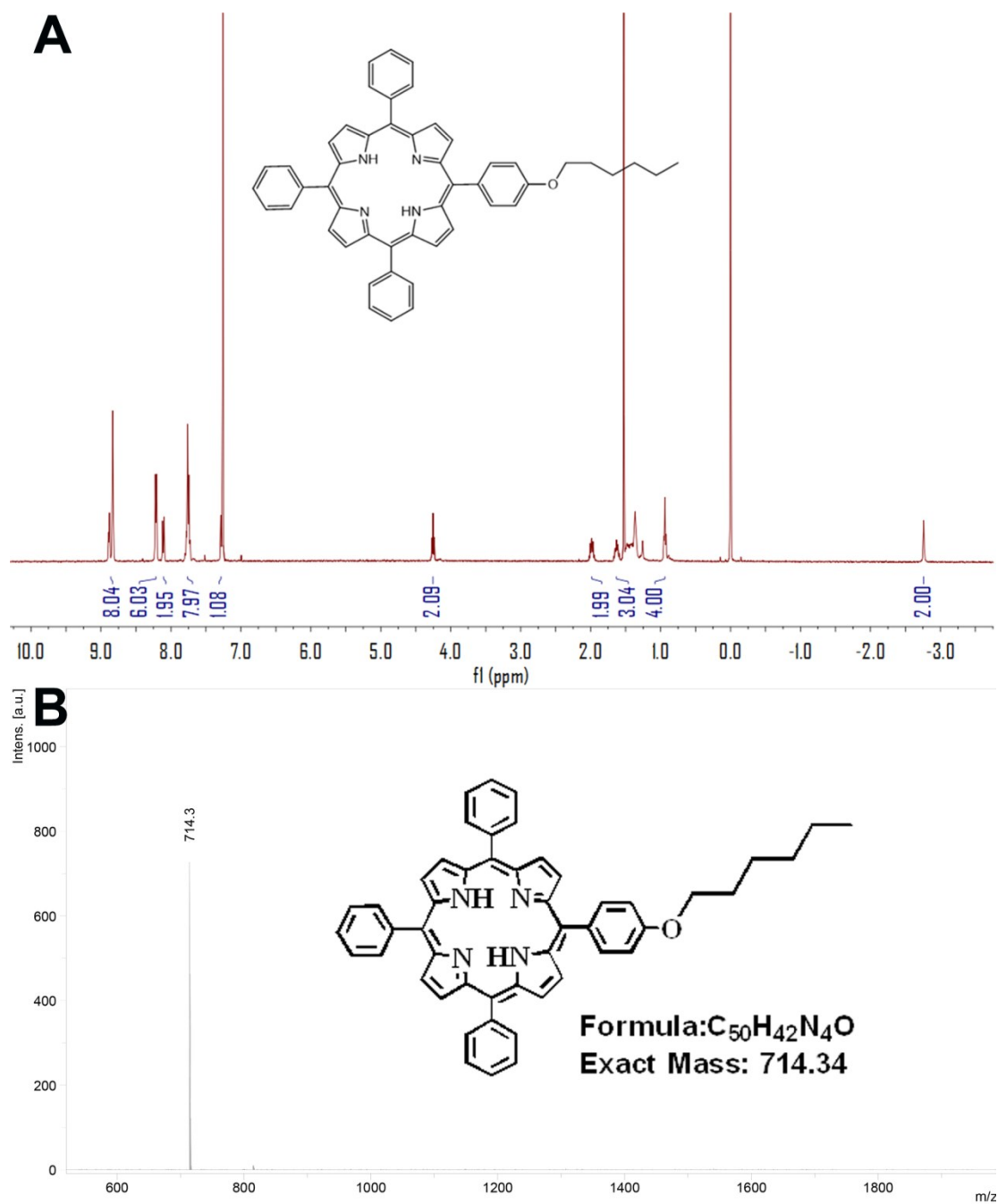


Fig. S4 (A) ¹H NMR spectrum of TPP-C₆ in CDCl₃. (B) MALDI-TOF mass spectrum of TPP-C₆.

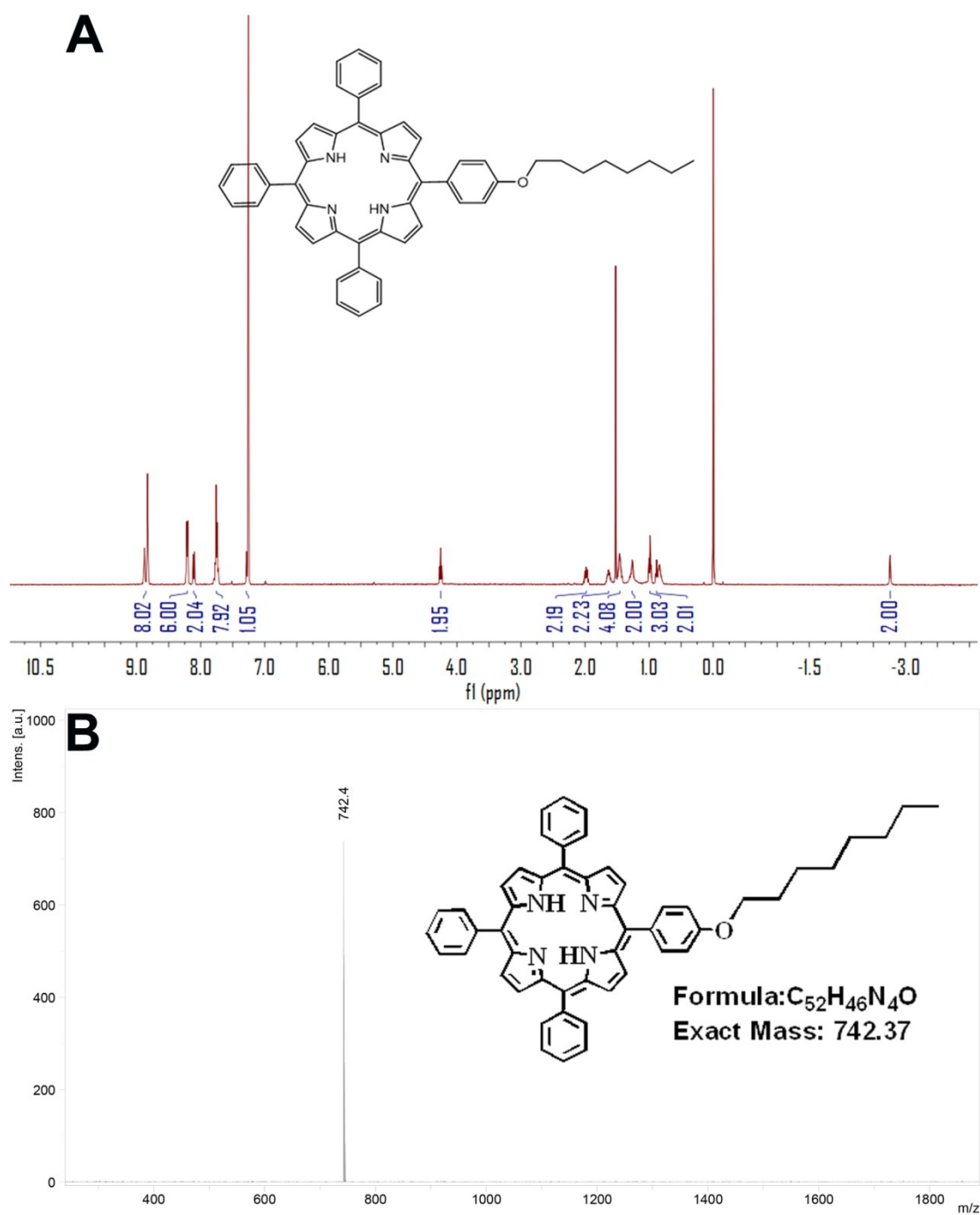


Fig. S5 (A) 1H NMR spectrum of TPP- C_8 in $CDCl_3$. (B) MALDI-TOF mass spectrum of TPP- C_8 .

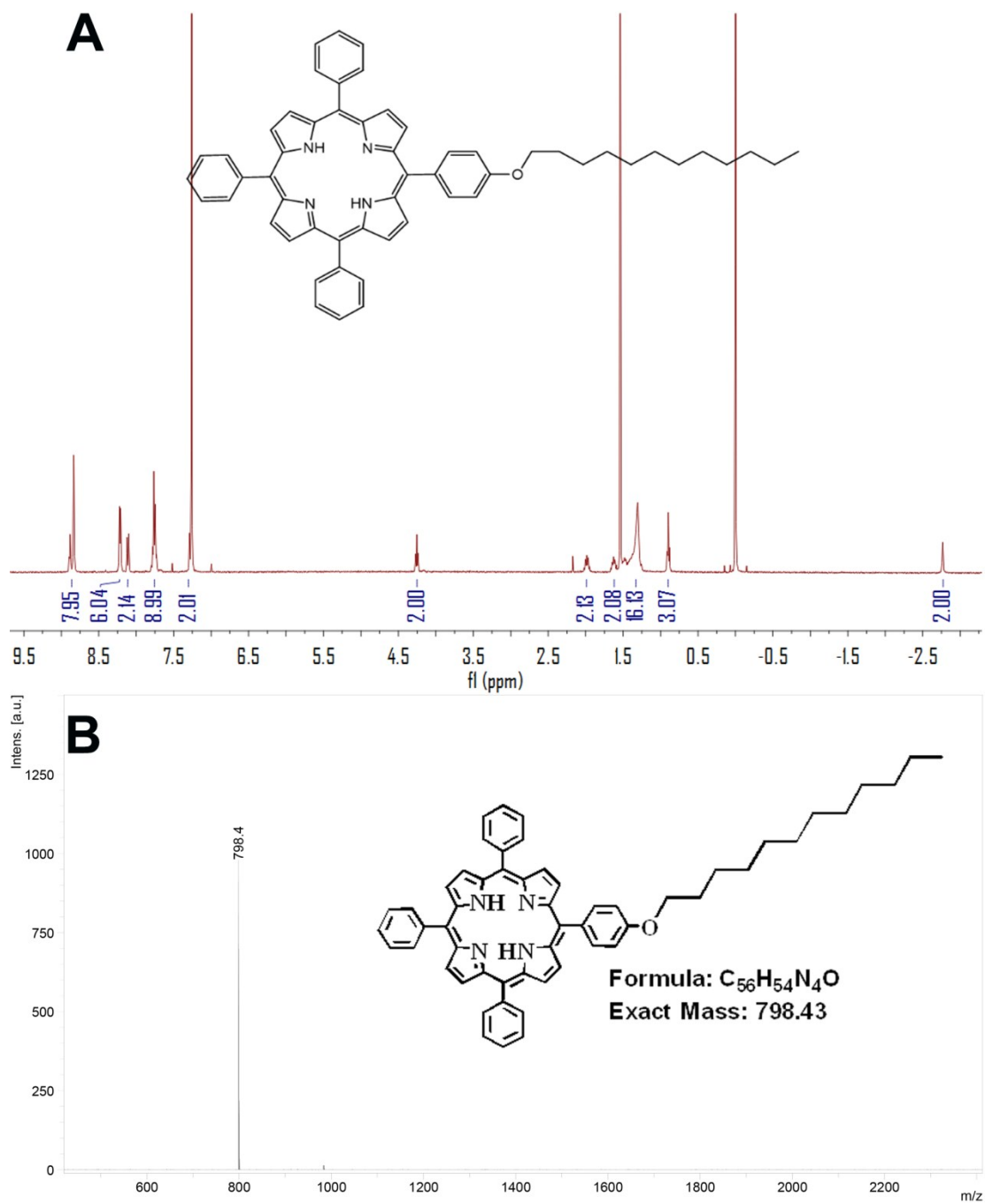


Fig. S6 (A) ¹H NMR spectrum of TPP-C₁₂ in CDCl₃. (B) MALDI-TOF mass spectrum of TPP-C₁₂.

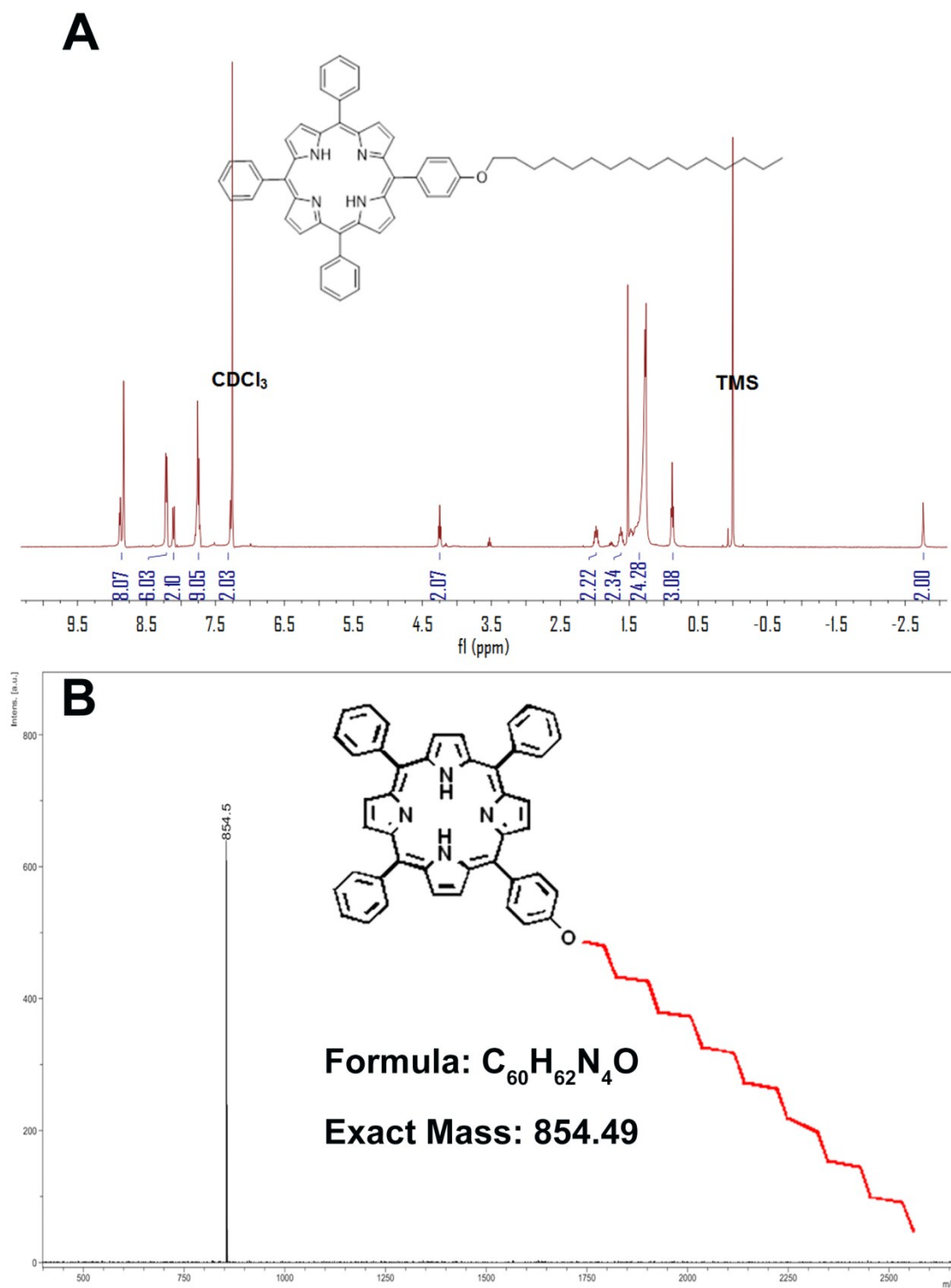


Fig. S7 (A) ¹H NMR spectrum of TPP-C₁₆ in CDCl₃. (B) MALDI-TOF mass spectrum of TPP-C₁₆.

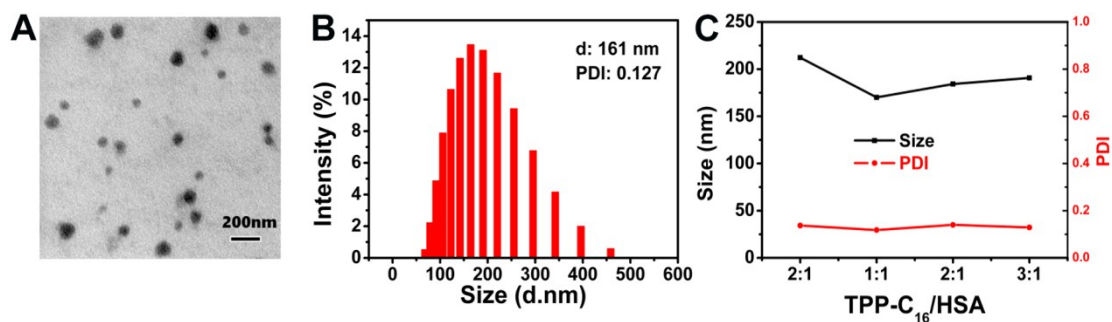


Fig. S8 (A) TEM image and (B) Size distribution of TPP-C₁₆ NPs. (C) The stability and PDI of TPP-C₁₆@HSA SNPs with different ratios of TPP-C₁₆/HSA.

Table S1 The particle size, PDI, and Zeta potential of different TPP-C_n@HSA SNPs.

| Sample ID (SNPs) | Average diameter (nm) | PDI | Zeta potential (mV) |
|--------------------------|--------------------------|-------------|------------------------|
| TPP-C ₂ @HSA | 150.3±0.35 | 0.143±0.021 | -32.7±0.5 |
| TPP-C ₄ @HSA | 167.1±4.0 | 0.164±0.031 | -21.3±0.96 |
| TPP-C ₆ @HSA | 165.8±0.5 | 0.121±0.019 | -30.9±0.7 |
| TPP-C ₈ @HSA | 155.7±0.1 | 0.131±0.001 | -20.0±0.08 |
| TPP-C ₁₂ @HSA | 185.9±0.8 | 0.129±0.04 | -28.6±0.5 |
| TPP-C ₁₆ @HSA | 177.0±0.1 | 0.169±0.004 | -30.03±0.4 |

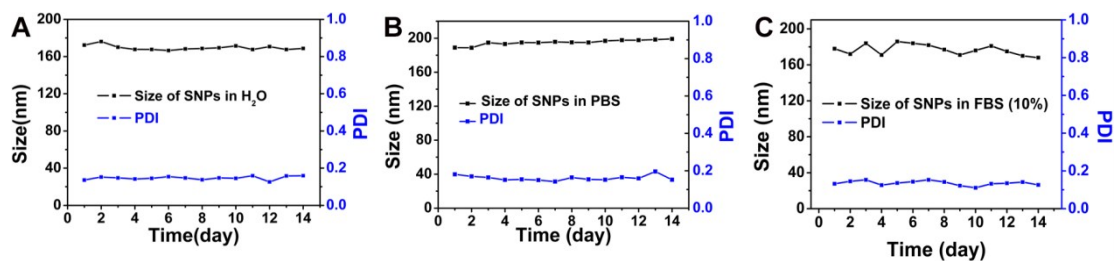


Fig. S9 DLS change profiles of TPP-C₁₆@HSA SNPs in (A) water, (B) FBS and (C) water containing 10% FBS for 14 days.

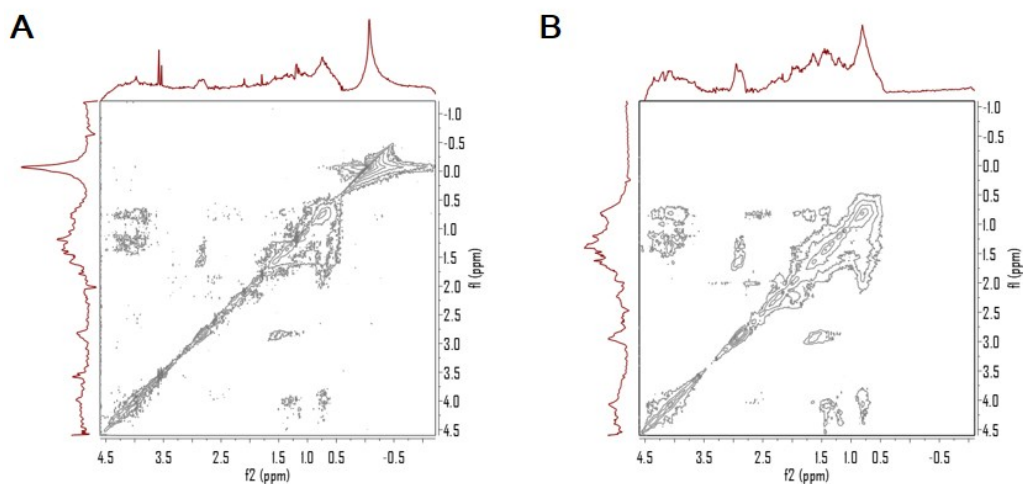


Fig. S10 2D NOESY spectra of (A) TPP-C₁₆@HSA and (B) HSA in D₂O at 298K with a mixing time of 400 ms.

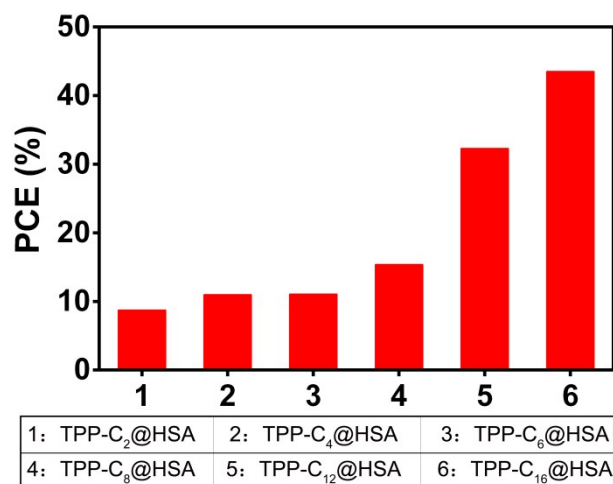


Fig. S11 The calculated photothermal conversion efficiency (PCE) results of TPP-C_n@HSA under the same conditions.

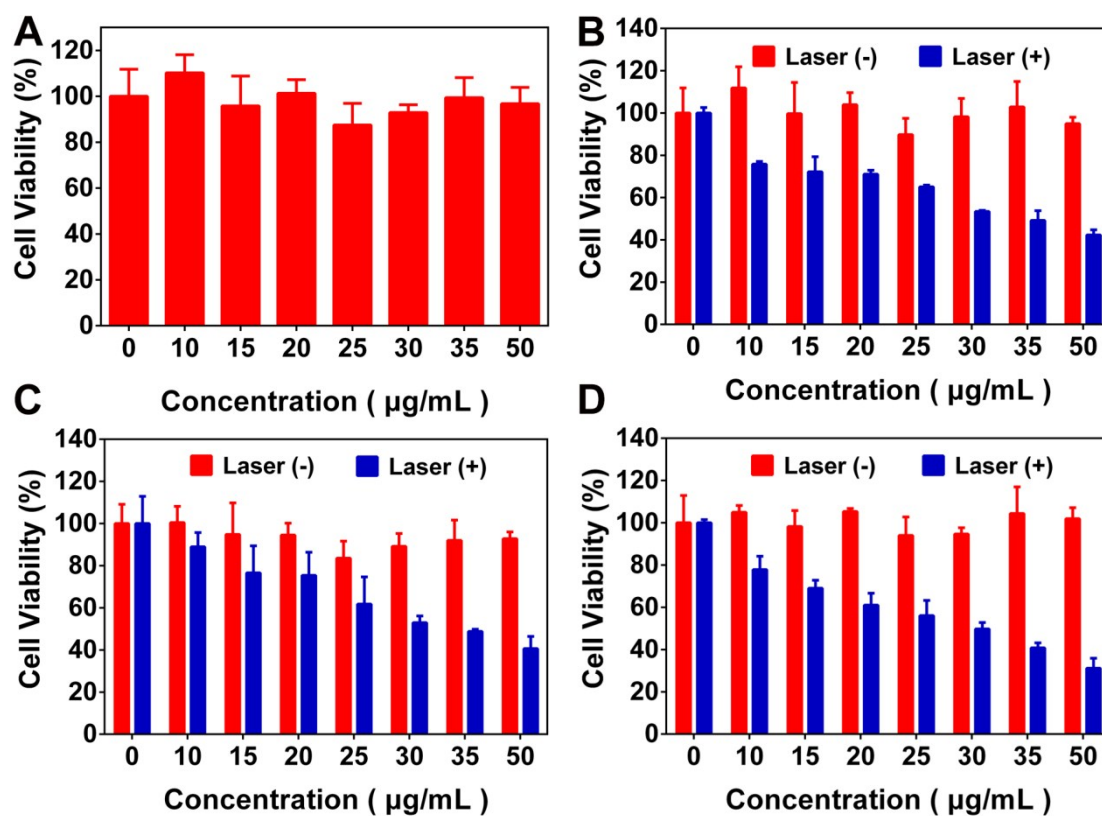


Fig. S12 *In vitro* cytotoxicity of TPP-C₁₆ NPs against (A) L929 cells without irradiation, (B) HeLa, (C) HepG2 and (D) U14 cells with or without laser irradiation (638 nm, 0.9 W cm⁻², 5 min).

Table S2 IC₅₀ Values of TPP-C₁₆ NPs and TPP-C₁₆@HSA SNPs against HeLa, HepG2 and U14 Cells.

| IC ₅₀ /µg mL ⁻¹ | HeLa | HepG2 | U14 |
|---------------------------------------|-------|-------|-------|
| TPP-C ₁₆ | 36.64 | 35.54 | 30.77 |
| TPP-C ₁₆ @HSA | 29.83 | 31.69 | 25.22 |

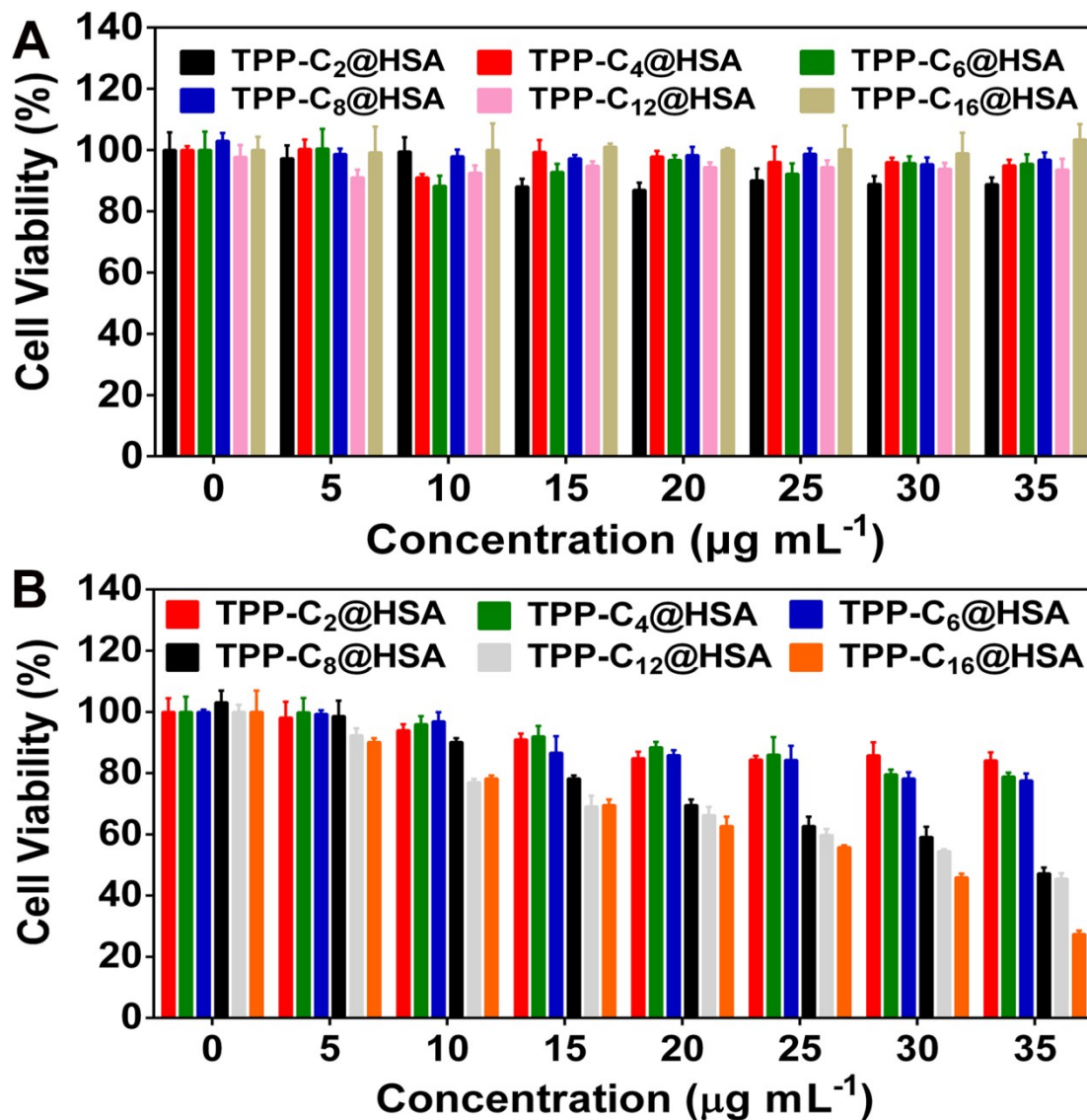


Fig. S13 The cell viability after incubated with TPP-C_n@HSA and treated (A) without irradiation or (B) with irradiation.

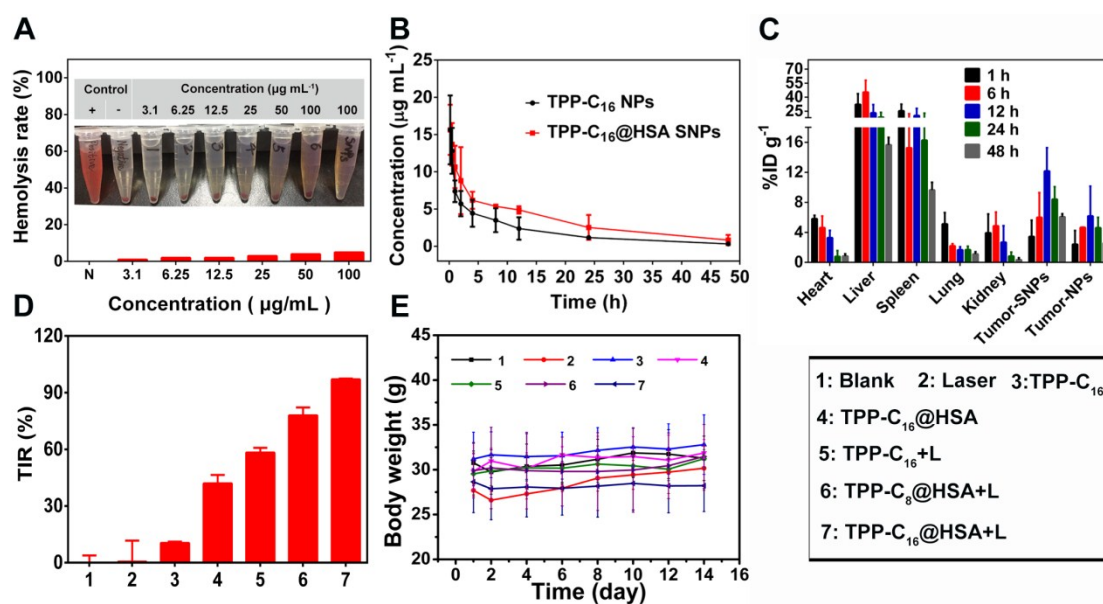


Fig. S14 (A) Hemolytic activity of different concentration of TPP-C₁₆@HSA SNPs. (B) The blood circulation of TPP-C₁₆@HSA SNPs and TPP-C₁₆ NPs at different time points after intravenous injection (n = 5). The area under curve (AUC) of TPP-C₁₆ NPs and TPP-C₁₆@HSA SNPs are 93.42 and 164.3, respectively. (C) The concentration of TPP-C₁₆ in the main organs and tumors at different time points after intravenous injection of TPP-C₁₆@HSA SNPs. Error bars represent standard deviation (n = 3). (D) The tumor inhibition rates (TIR) and (E) body weight changes of mice from different groups.

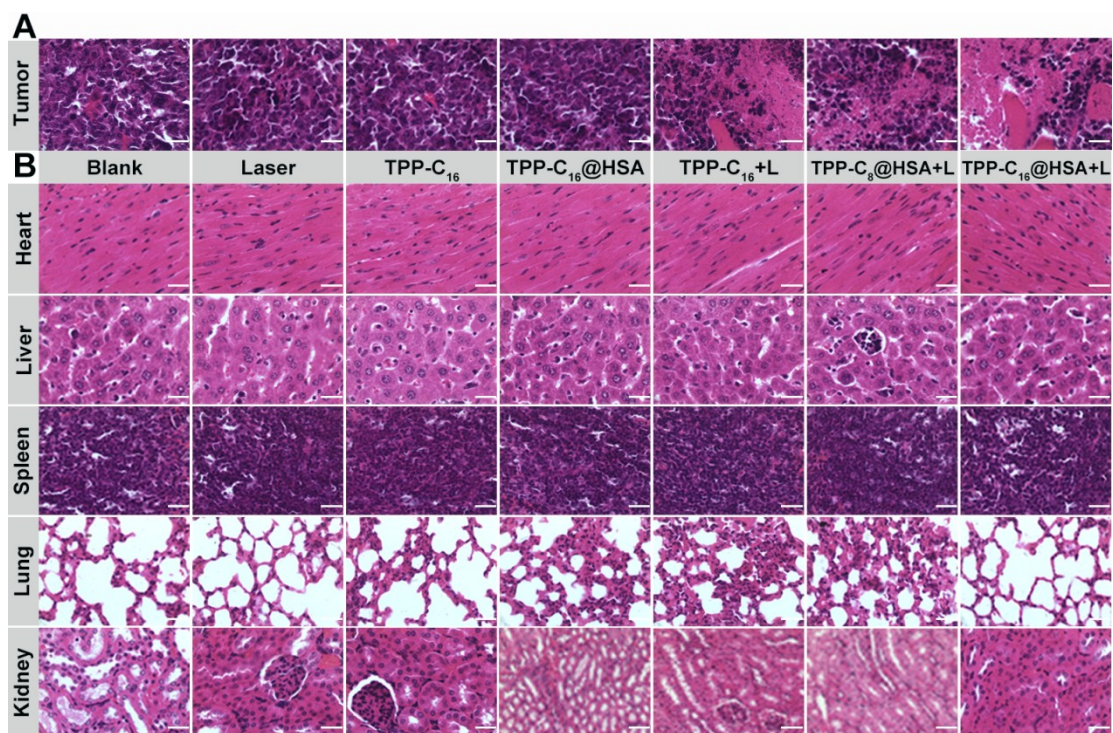


Fig. S15 (A) H&E staining photos of tumor slices in different groups made by a microscope. (B) H&E staining pictures of the main organ slices obtained from the seven groups. Scale bars: 100 μm.